

Review

Recent Advances in Acoustics of Transitional Airfoils with Feedback-Loop Interactions: A Review

Vladimir Golubev

Department of Aerospace Engineering, Embry-Riddle Aeronautical University, Daytona Beach, FL 32114, USA; vladimir.golubev@erau.edu

Abstract: We discuss herein recent experimental and numerical studies examining resonant flow-acoustic feedback-loop interactions in transitional airfoils (i.e., possessing a notable area of laminar-to-turbulent boundary-layer transition) characteristic of low-to-medium Reynolds number flow regimes. Such interactions are commonly attributed to the viscous dynamics of the convected boundary-layer structures scattering into acoustic waves at the trailing edge which propagate upstream and re-excite the convected vortical structures. While it has been long suspected that the acoustic feedback mechanism is responsible for the highly pronounced, often multi-tonal response, the exact reason of how the boundary-layer instability structures could reach a sufficient degree of amplification to sustain the feedback-loop process and exhibit specific tonal signature remained unclear. This review thus pays particular attention to the critical role of the separation bubble in the feedback process and emphasizes the complementary roles of the experimental and numerical works in elucidating an intricate connection between the airfoil radiated tonal acoustic signature and the properties of the separation zones as determined by airfoil geometry and flow regimes.

Keywords: airfoil self-noise; acoustic feedback loop (AFL); laminar separation bubble (LSB); leading edge (LE) and trailing edge (TE); boundary layer (BL); Tollmien–Schlichting (T-S) and Kelvin–Helmholtz (K-H) instabilities; high-fidelity numerical analysis; theoretical analysis; experimental study



Citation: Golubev, V. Recent Advances in Acoustics of Transitional Airfoils with Feedback-Loop Interactions: A Review. *Appl. Sci.* **2021**, *11*, 1057. <https://doi.org/10.3390/app11031057>

Academic Editor: Jens Nørkær Sørensen
Received: 29 December 2020
Accepted: 15 January 2021
Published: 25 January 2021

Publisher's Note: MDPI stays neutral with regard to jurisdictional claims in published maps and institutional affiliations.



Copyright: © 2021 by the author. Licensee MDPI, Basel, Switzerland. This article is an open access article distributed under the terms and conditions of the Creative Commons Attribution (CC BY) license (<https://creativecommons.org/licenses/by/4.0/>).

1. Introduction

The unusual unsteady response of transitional airfoils subjected to moderate Reynolds number (Re) flows has been studied for nearly half a century since the pioneering experimental work by Paterson et al. [1]. Nevertheless, the controversy surrounding the interpretation of physical mechanisms triggering such response still persists, largely due to the high sensitivity of the transitional airfoil response to minute changes in flow conditions. For instance, in a recent study by Tank et al. [2] correlating lift and drag measurements collected from multiple wind-tunnel and computational experiments, the findings proved to be highly contradictory due to the sensitive nature of the transitional airfoils and the resulting abrupt changes in airfoil response associated with it. Efforts to control such sensitivity using acoustic forcing to help improve aerodynamic performance have been attempted experimentally by Yang et al. [3]. Earlier, the same technique was employed computationally by Jones et al. [4] to examine the boundary-layer receptivity in the process of establishing the acoustic feedback loop (AFL) resulting in possibly the most distinct signature of the transitional airfoils, the highly pronounced tonal noise radiation with characteristic dual-ladder type frequency spectrum structure.

The transitional airfoil's tonal noise signature was first comprehensively presented by Paterson et al. [1]. Through experimental testing, they successfully investigated the acoustics emitted by symmetric NACA airfoils in the Re range corresponding to full-scale helicopter rotors. Their key finding (reproduced in Figure 1) shows an unusual ladder-type structure (staging) of tones wherein the peak frequencies are scaled $\sim U^{1.5}$ (U is the freestream velocity) with sudden jumps appearing between the rungs of the ladder scaled $\sim U^{0.8}$. During this effort, Paterson et al. [1] successfully correlated the relationship

between the peak tonal frequencies with the natural vortex shedding characteristics of the airfoil, which scaled at $\sim U^{1.5}$. However, the reason for the tones scaling with $\sim U^{0.8}$ was at that time still unknown. Subsequently, Tam [5] suggested his version of the acoustic feedback-loop (AFL) mechanism to explain the tonal staging. The proposed AFL consists of unstable laminar separation bubbles (LSBs) on both the pressure and suction sides of the airfoil merging at the trailing-edge (TE) to form the unsteady near-wake sheared flow profile. As the flow is convected from the sharp TE, the naturally occurring disturbances (free-shear K-H instabilities) resulting from the vortex shedding develop and amplify until their amplitudes become sufficiently large to manifest as tonal acoustic source. At this moment, the generated sound waves propagate in all directions, but most importantly, convect upstream and interact with induced TE instabilities. This interaction of the upstream-propagating acoustic waves and TE instabilities force the boundary layer (BL) to oscillate resulting in further amplification of the initial disturbances and subsequent tonal acoustic emission. The process is then repeated to complete the AFL. Interestingly, while such an AFL scenario was later rejected, Tam and Ju [6] have recently re-visited the problem to propose the TE scattering of near-field wake K-H instability as the primary source of the vortex-shedding self-noise generation mechanism for low- Re airfoils with distinct shedding-tone signature, as further discussed below.

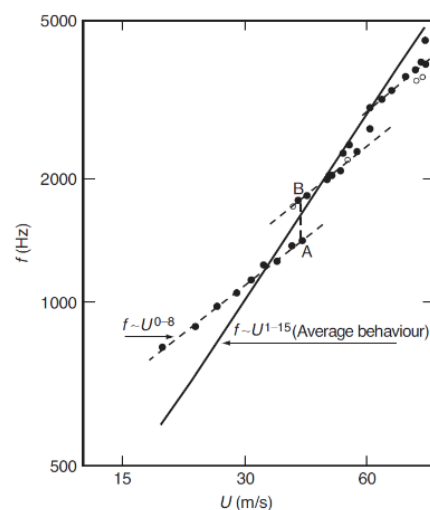


Figure 1. Airfoil ladder-type frequency structure (adapted from Paterson et al. [1]).

Tam's [5] AFL scenario was later re-visited by Longhouse [7] who suggested a different perspective on the feedback-loop mechanism based on the hypothesis of Fink [8] and Schlinker and Amiet [9]. Instead of considering the AFL to occur in the wake, Longhouse [7] hypothesized that the process actually began very early on the airfoil surface. As illustrated in Figure 2, the proposed AFL appears as a result of instabilities incepted near the airfoil's leading-edge (LE) in the form of T-S waves. Due to the natural flow convection, the T-S waves were presumed to have sufficient time to amplify in strength as they approached the TE where they scattered into noise. This scattering mechanism, in addition to the airfoil natural vortex shedding, generated the acoustic waves propagating upstream to induce the BL vortical disturbances through the receptivity mechanism. In the established AFL process, the phase of the upstream-propagating acoustic wave must match the phase of the downstream-traveling instability waves so that a stronger acoustic wavefront could be deployed upstream to maintain the feedback loop.

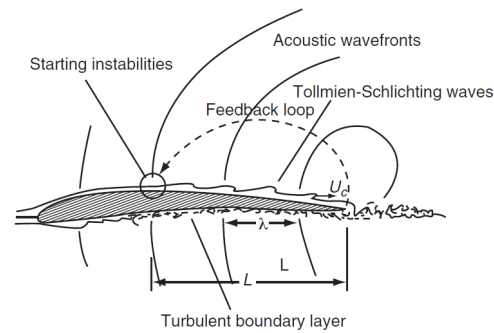


Figure 2. Feedback loop in airfoil flow-acoustic interaction (adapted from Longhouse [7]).

The AFL scenario proposed by Longhouse [7] was further elaborated by Arbey and Bataille [10] based on a series of experiments with NACA-0012 airfoils. Their recorded acoustic spectra generally confirmed the tonal ladder-type structure of Paterson et al. [1] to produce, for a given velocity in the range of $U = 20 \dots 40$ m/s ($Re_c = 2 \dots 6 \times 10^5$), a narrowband set of equidistant frequencies superimposed on a broadband hump (Figure 3). In agreement with the interpretation suggested by Longhouse [7], Arbey and Bataille [10] concluded that such contribution was indeed attributed to T-S instability waves developing in BL and scattering as sound at the airfoil TE. The AFL was presumed generated between selected TE-radiated acoustic waves and the most amplified T-S waves based on the condition that both acoustic and convected instability waves are in phase at the point of the instability inception. Furthermore, Arbey and Bataille [10] proposed the first explanation for the tonal ladder staging of Paterson et al. [1] by correlating the $U^{0.8}$ velocity dependence with diffraction of T-S instabilities at the airfoil TE. To supplement their measured data, the linear stability theory (LST) and a modified version of Tam's [5] AFL formula were employed to predict the peak and discrete frequencies, with results showing a good agreement, which further validated their findings.

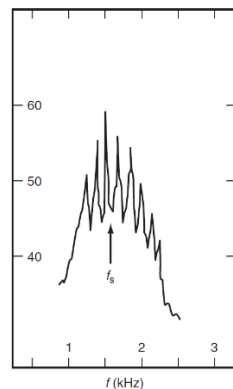


Figure 3. Airfoil frequency spectrum (adapted from Arbey and Bataille [10]).

The early works on the subject of tonal noise produced by transitional airfoils (reviewed, e.g., in Nash et al. [11], Kingan and Pearse [12], Plogmann et al. [13], Golubev et al. [14], Tam and Ju [6], and Yakhina et al. [15]) discussed AFL as the necessary and sufficient condition for generation of the airfoil tonal noise. Such discussion was particularly focused on the controversies observed between results of different experimental studies, which in some instances failed to observe the ladder-type acoustic tonal structure. Some authors, including Nash et al. [11] and Tam and Ju [6], rejected the idea of the feedback loop (in the sense proposed by Longhouse [7]) as a pre-requisite for airfoil tonal self-noise, while attributing other experimental claims to various installation effects. In their DNS study of NACA-0012 airfoil, Tam and Ju [6] observed only a single shedding tone, and at much lower amplitude compared to some other experimental and numerical studies.

They also demonstrated correspondence of the shedding frequency tone to TE-scattered most amplified near-wake K-H instability. However, their simulations were conducted for NACA-0012 airfoil at zero AoA with fully laminar flow conditions, with no LSB and AFL present. They also rightfully pointed to the fact that viscous T-S instabilities themselves are slowly growing and would not have sufficient magnitudes to produce a significant acoustic radiation through TE scattering.

On the other hand, a number of investigators including Desquesnes et al. [16] and Jones et al. [4] employed direct numerical simulations (DNS) and linear stability analysis in transitional regime to elaborate on AFL genesis including BL receptivity and tonal frequency selection process. With the primary radiated tone corresponding to the shedding frequency rather than the most amplified BL instability mode, Jones et al. [4] suggested that AFL plays a role in frequency selection for the vortex shedding that occurs naturally. Later, Jones and Sandberg [17] argued that while vortex shedding occurs naturally in the absence of AFL, the latter when present may act as a frequency selection mechanism for the pre-existing vortex shedding behavior. They agreed with Tam and Ju [6] that a sustained AFL should depend upon large convective instability growth rates within the airfoil BL in order to overcome the energy losses incurred via the trailing-edge scattering and BL receptivity processes, and further hypothesized that if sustained, the feedback loop could impart a greater regularity to the vortex shedding behavior thus leading to a more pronounced narrow-band (i.e., tonal rather than broadband) energy content. The AFL regulated tonal amplitudes would then be expected at much higher amplitudes compared to the pure laminar shedding tone of Tam and Ju [6].

Overall, the complex interaction between AFL and vortex shedding mechanisms manifesting itself in the dual-ladder frequency staging of tones became one of the critical issues addressed in the recent studies. In the last decade, there has been a significant breakthrough in understanding the airfoil feedback loop process, to a large degree based on realizing the importance of the separation bubble and its position on the airfoil surface as determined by the airfoil flow regime. The frequency selection process that determines the ladder-type acoustic tonal structure has been identified with the help of high-fidelity studies and linear stability theory. In this regard, the complementary roles of concurrent experimental and numerical studies are of particular importance, as emphasized in the discussion below.

The review is organized as follows. In Section 2, we address the investigated mapping of the flow regimes where the tonal airfoil self-noise signature was identified in various experimental studies. This provides with the reference point for the further analysis of numerical predictions detailing the underlying physics of transition from tonal- to non-tonal-producing flow regimes. Note that almost all such mapping studies consider a symmetric NACA-0012 airfoil. In addition, Yakhina et al. [15] and Nguyen et al. [18] considered a cambered SD7003 airfoil in their complementary experimental and numerical works, with the more detailed review of their concurrent investigations included in Section 3 addressing the effect of separation bubble properties in connection with produced airfoils tonal signature recorded or predicted at various flow regimes. Finally, Section 4 examines a critical aspect of frequency selection in the tonal spectrum, with the ladder-type structure traced to a complex nonlinear interaction of TE shedding and feedback-loop mechanisms.

2. Tone-Producing Flow Regimes

Parametric experimental studies conducted by Paterson [1], Arbey and Bataille [10], Lowson et al. [19], and later by Arcondoulis et al. [20] analyzed acoustic data for NACA-0012 airfoil in order to map the regions of discrete tones in the angle-of-attack (AoA) vs. Re plane (Figure 4). In some of these studies, T-S waves were observed at the lower Re than the one corresponding to the first tone appearance. In other words, T-S instabilities alone were not a sufficient condition for the occurrence of the acoustic radiation and/or the feedback process. Instead, such a process was associated with the presence of a separation

bubble at the airfoil pressure side, while the sound intensity was correlated with the length of the bubble.

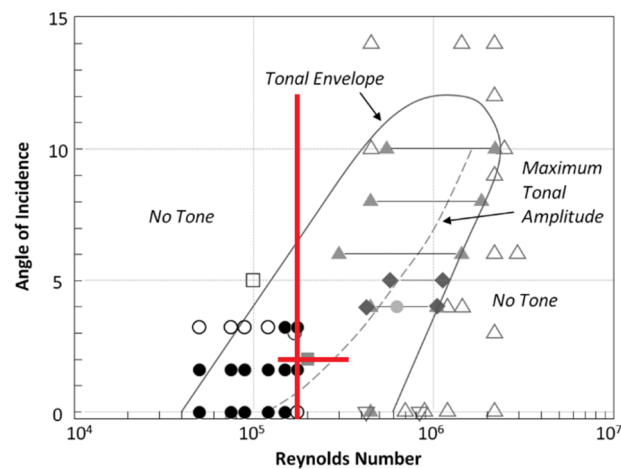


Figure 4. Integrated plot adapted from Lawson et al. [19] and Arcondoulis et al. [20] indicating NACA-0012 tone-producing and no-tone-producing regions according to experimental and numerical studies of Desquesnes et al. [16] (squares), Lawson et al. [19] (diamonds), Arcondoulis et al. [20] (circles), Paterson et al. [1] (triangles), and Arbey and Bataille [10] (inverted triangles). Filled markers represent tone-producing regimes, while unfilled markers represent no-tone-producing regimes. Tonal envelope and maximum tonal amplitude (dashed) line are from experiments by Lawson et al. [11]. Red lines indicate regimes investigated by Nguyen et al. [18].

Most recently, Yakhina et al. [15] reported on the results of a comprehensive experimental campaign where far-field sound-pressure measurements were recorded for NACA-0012 and SD7003 airfoils (compared in Figure 5) at various flow speeds and geometrical angles of attack. The tonal data obtained for NACA-0012 airfoil showed both similarities and differences with the previous studies, which suggests the high sensitivity of the AFL mechanism to experimental conditions. The cambered SD7003 airfoil was found to have a much narrower emission area than the NACA-0012. The measurements also confirmed the AFL-induced “ladder-type” structure featured when plotting the variation of the dominant tone with increasing flow speed, for both airfoils. Yakhina et al. [15] also categorized several regimes of tone emission, namely a switching regime between two tones that are not observed simultaneously, a regime with a single tone or two simultaneous tones, and a regime of intermittency with multiple unstable tones.

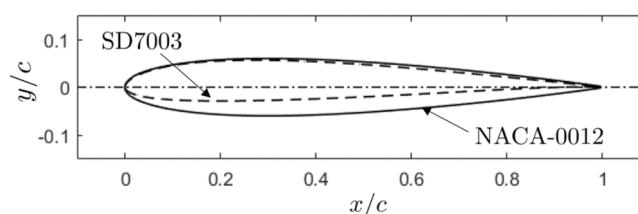


Figure 5. NACA-0012 and SD7003 airfoils employed in experimental study of Yakhina et al. [15].

Concurrently and in close collaboration with experimental efforts of Yakhina et al. [15], Nguyen et al. [18] conducted a series of high-fidelity numerical parametric investigations of the effects of AoA and Re that confirmed that the sustainment of AFL was dependent on the formation of LSB. Furthermore, using a combination of high-fidelity and linear stability analyses, they substantiated the switch from viscous T-S to inviscid K-H instabilities (facilitated by the presence of LSB near TE) as a necessary condition for AFL existence. These and some other recent studies are further detailed below in the discussion of the

investigation methods used and the physical mechanisms found responsible for the genesis of AFL and the observed transition between tone- and no-tone-producing regimes.

3. Laminar Separation Bubble and Acoustic Feedback Loop Process

As mentioned above, the controversy surrounding the mechanisms of airfoil tonal self-noise may be attributed to the highly sensitive nature of AFL process. Such sensitivity clearly reveals itself in the impact of experimental facilities on the measured tonal response that led some experimentalists like Nash et al. [11] to believe that AFL's dual ladder-type spectral feature is not an airfoil's intrinsic but rather a facility-induced phenomenon. However, most subsequent experimental works disagreed with such a conclusion by providing evidence of the tonal structure recorded and further investigated using the most advanced measurement techniques. Furthermore, with the advancement of modern computational capabilities, previously prohibitively expensive high-fidelity studies have been conducted that not only allowed to clearly confirm the natural existence of the AFL mechanism but enabled an in-depth analysis of the underlying physics through careful post-processing and correlation of airfoil-surface and far-field unsteady flow-field data statistics.

3.1. Experimental Approaches

In the last decade, a number of experimental studies explored NACA-0012 airfoil tonal noise in the transitional flow regimes (e.g., [13,15,20–26]), with nearly all reporting a connection between observed LSB and the tonal noise generation. Tools such as particle image velocimetry (PIV) and surface oil visualization were commonly used, along with surface and far-field unsteady pressure measurements. With the use of time-resolved analysis, the BL vortical structures showed a strong spanwise and streamwise coherence with the vortex shedding frequency at the trailing edge. The localization of the separation zone in parametric experiments was found to strongly depend on AoA and Re , with the suction-side or pressure-side dominating the tonal noise emission for NACA-0012 airfoil at low and high Reynolds numbers, respectively [15,21,23]. Separation areas were also reported as amplifiers for the instability waves [15,22–24]. The authors also confirmed a ladder-type structure compatible with the power laws identified by Paterson et al. [1].

Using NACA-0018 airfoil, Gerakopulos and Yarusevych [27] used time-resolved wall-pressure measurements and hot-wire anemometry to investigate LSB. They observed a strong correlation between velocity fluctuations in the separated shear layer and wall-pressure fluctuations, and deduced values of the convection speed of the instabilities from measurements on pairs of wall microphones. Such information is later employed in theoretical predictions of AFL-selected tonal frequencies matched with the recorded far-field tonal noise spectrum.

Perhaps the most comprehensive and careful (from the standpoint of isolating facility interference effects) experimental measurements of the decade were carried out in an anechoic low-speed wind tunnel facility at Ecole Centrale de Lyon (ECL), with the exhaustive details of the experimental campaign described in Yakhina et al. [15] and briefly reviewed below as an example of the advanced experimental approaches. The tonal signature of the low-speed NACA-0012 and SD-7003 airfoils was examined for a range of transitional flow regimes characterized by variable inflow velocity (5 ... 40 m/s, corresponding to $Re = 0.4 \times 10^5 \dots 3.2 \times 10^5$), AoA ($-15^\circ \dots 15^\circ$), and unsteady inflow conditions to allow for thorough mapping of the regions of tonal production including effects of upstream unsteadiness. The issues raised by Nash et al. [11] related to possible installation effects producing ladder-type tonal structure motivated a new design of the mounting device compared to the first stage of the experimental campaign described in [14]. The employed configuration minimizes spurious reflections from end-plate surfaces used in most experimental setups described in the literature and ensures that upstream-propagating sound from the TE is the only mechanism of acoustic excitation for instabilities. The new design was tested and confirmed that larger end plates produced no impact on the results. The ladder-type structure of the acoustic signature was thus believed intrinsic to the develop-

ment and radiation of instability waves in the transitional flow. The only possible remaining installation effect is the jet-flow deflection due to lateral momentum injection associated with the mean lift as the airfoil is set at a non-zero AoA. However, this was not believed to significantly modify the underlying physics of the observed phenomena. Far-field acoustic measurements performed in the mid-span plane using a single microphone on a rotating arm provide an overview of frequency-angle characterization and spectral directivity of the sound. To correlate acoustics with wall-pressure fluctuations, an elaborate technique of measurements using remote-microphone probes (RMPs) flush mounted along the airfoil surface was employed (see Figure 6).

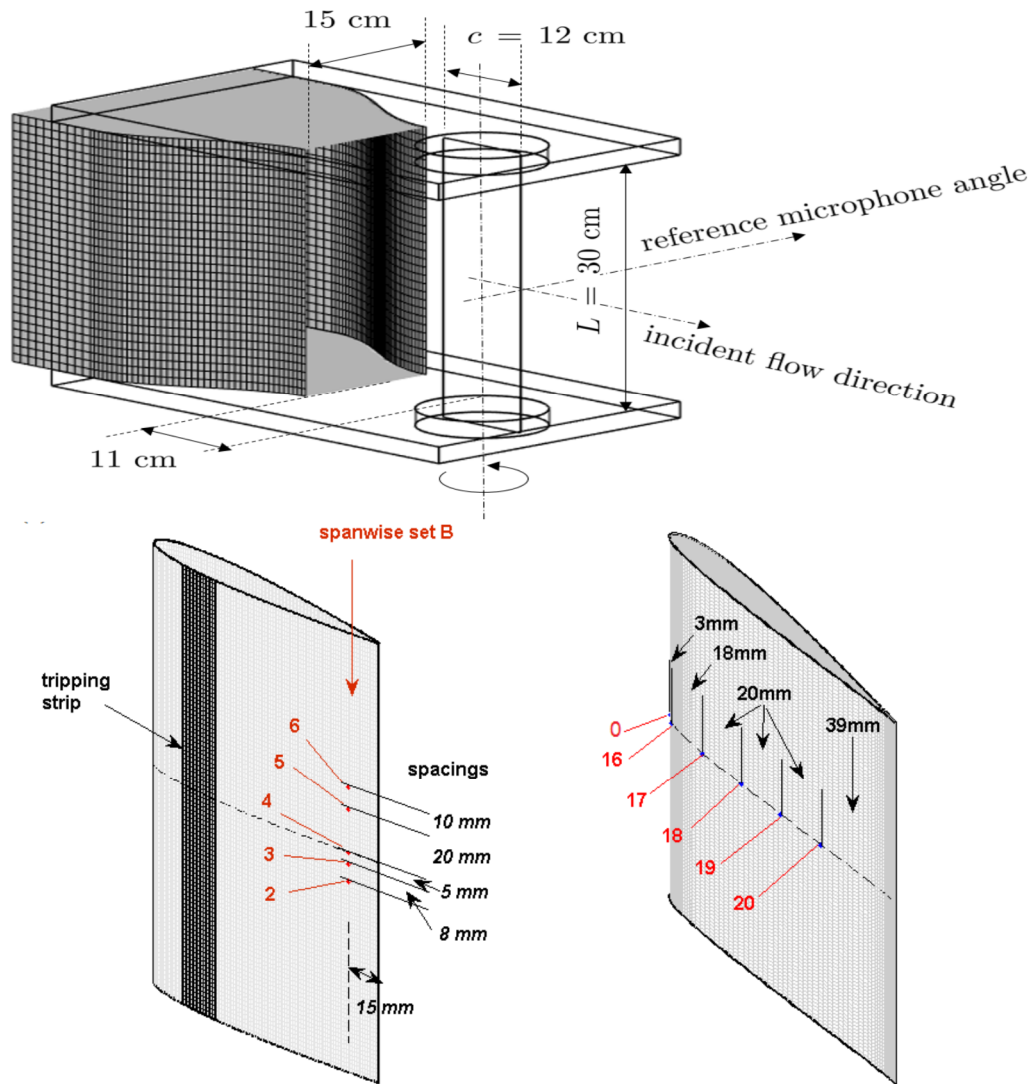


Figure 6. Sketch of the experimental setup used by Yakhina et al. [15] illustrating pin-hole locations and probe labels of the wall-pressure Remote Microphone Probes (RMP) on the NACA-0012 (bottom left) and SD7003 (bottom right) mock-up.

Classical hot-wire anemometry (HWA) and oil-visualization of the flow were used to identify LSB zones involved in the tonal noise mechanism and their dynamics with changing flow velocity and AoA. In addition, to explore the effect of internal and external BL excitations on LSB, AFL, and the resulting trailing-edge noise, both a surface tripping device and an upstream turbulence grid were employed. Several configurations with tripping devices added on one side or the other, as well as on both sides, have been tested, with the tripping device represented by a strip of medical adhesive plaster located around the expected area of maximum local velocity (Figure 6). The tripping forces transition of

the laminar boundary layer to turbulence and deactivates the generation of tonal noise. The influence of a fine-scale homogeneous upstream turbulence was studied by inserting a turbulence grid before the wind tunnel nozzle contraction (top of Figure 6).

Figure 7 illustrates results of the far-field sound measurements obtained in [15] and presented in the form of a color-level map, with the frequency and flow speed as coordinates in logarithmic scales. The results are plotted for NACA-0012 airfoil at $AOA = 0^\circ$, and for SD7003 airfoil at $AOA = 2^\circ$ (which geometrical AOA corresponds to the zero effective AOA). The dominant tones at each measured flow speed are marked by red symbols. Clearly, these results feature the ladder-type structure discussed by previous investigators [1,10,13,25,26] with the dual dependence attributed to shedding and AFL mechanisms to be further addressed below.

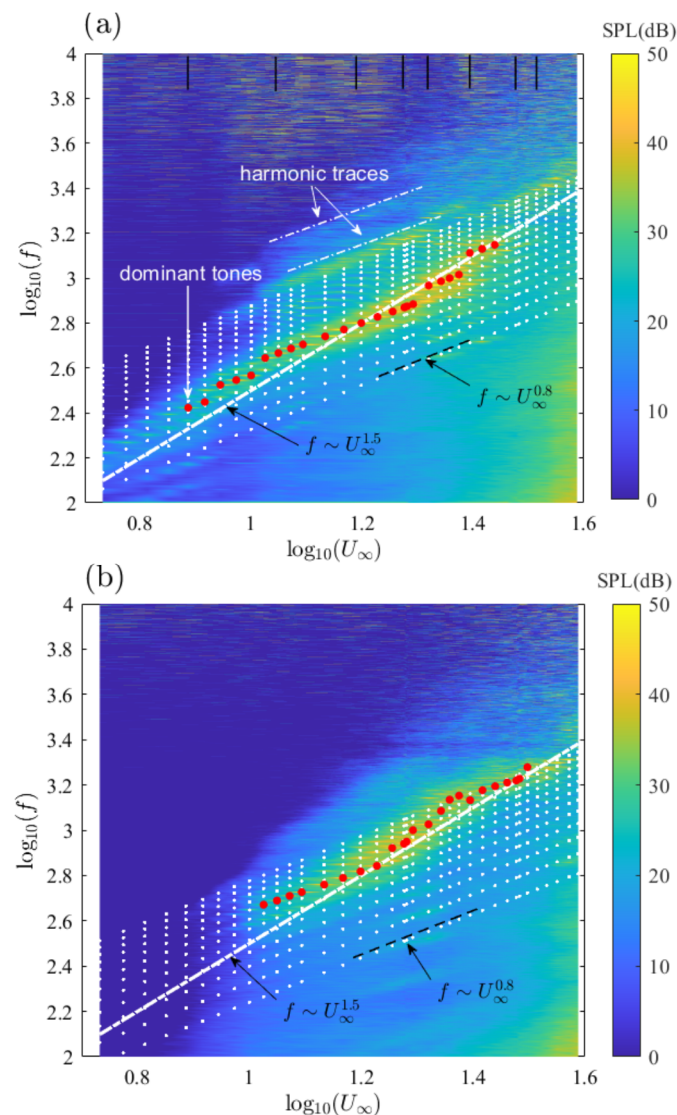


Figure 7. Frequency-flow speed maps of noise radiation for clean airfoils: NACA-0012 at zero AOA (a), SD7003 airfoil at 2° geometrical AOA (b) [15].

Sound spectra for SD7003 airfoil extracted from the map in Figure 7b at some indicative flow speeds are shown in Figure 8 revealing zones of multiple-tone generation. A detailed spectrogram analysis in [15] showed non-stationary properties of the acoustic signals observed for both airfoils. In particular, regimes with a single dominant tone, two tones, switching tones, and a regime with intermittent tonal radiation were identified.

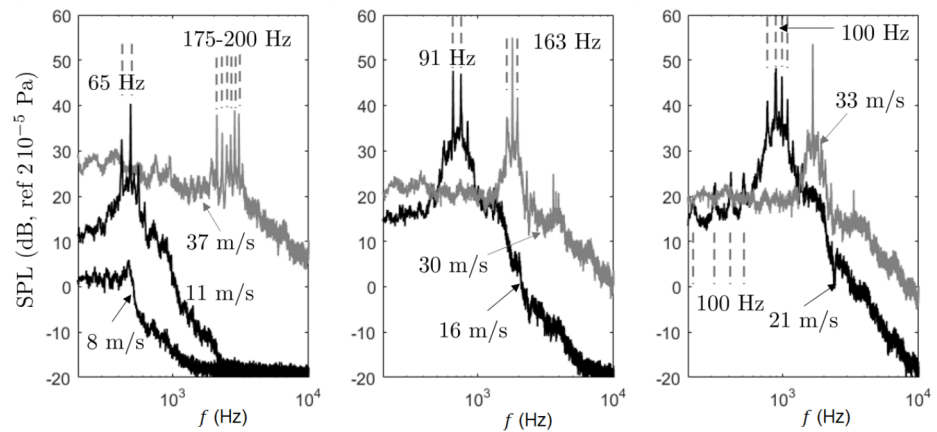


Figure 8. Sound-pressure spectra extracted from the map in Figure 7b showing multiple tones for SD7003 airfoil at various flow speeds (presented in three plots for clarity). Values of the averaged frequency jumps for series of tones indicated on the plots (dashed vertical segments) [15].

Tracking the position of LSB zones on either side of the airfoil with tonal radiation pattern, the noise emission areas in the AOA-*Re* plane were constructed, as shown in Figure 9a for both airfoils and compared in Figure 9b with previous results reported in Figure 4. Note that the emission area for SD7003 airfoil is very narrow in terms of the effective AOA, thus the results are presented for geometrical AOA in Figure 9a. Compared to the filled circles bordering the area of AFL-induced tonal radiation, the empty circles indicate the onset of a low-amplitude noise corresponding to some primary emission free of AFL. In agreement with Pröbsting et al. [22], the emission area for NACA-0012 airfoil features two sub-regions: At low *Re*, the tones are produced by the suction-side BL whereas at higher *Re* they are produced by the pressure-side BL. These results will be further elaborated later in comparison with numerical predictions.

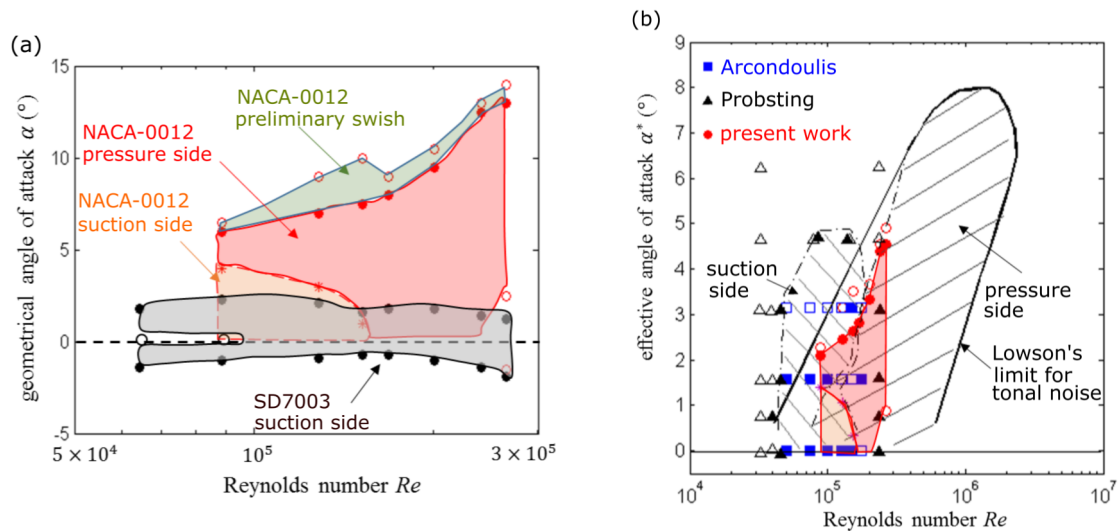


Figure 9. (a) Geometrical angle-of-attack (AOA) vs. *Re* tonal noise map from [15] for NACA-0012 and SD7003 airfoils. Filled circles show the limits of the tonal-noise regime; empty circles point to the onset of low-amplitude noise. Green area is the primary emission for the NACA-0012 airfoil, red and orange areas are tonal noise generated by pressure or suction sides of the NACA-0012, respectively, and grey area is tonal noise generated by suction side of SD7003 airfoil. (b) Effective AOA vs. *Re* tonal noise map from [15] for NACA-0012 airfoil, compared with previous investigations (see also Figure 4).

The effect of upstream turbulence grid on the frequency-vs.-flow speed map measured with NACA-0012 airfoil at zero AOA is plotted in Figure 10a. With the AFL mechanism

suppressed, neither ladder-type structure nor tonal noise is observed (as in Figure 7a) but the map exhibits an oblique trace with the primary scaling law $\sim U^{1.5}$ characteristic of a broadband shedding hump in airfoil self-noise spectrum. This is further illustrated in Figure 10b where the sound spectra for upstream velocities of 8 m/s and 25 m/s are compared in clean-flow and grid-turbulence conditions.

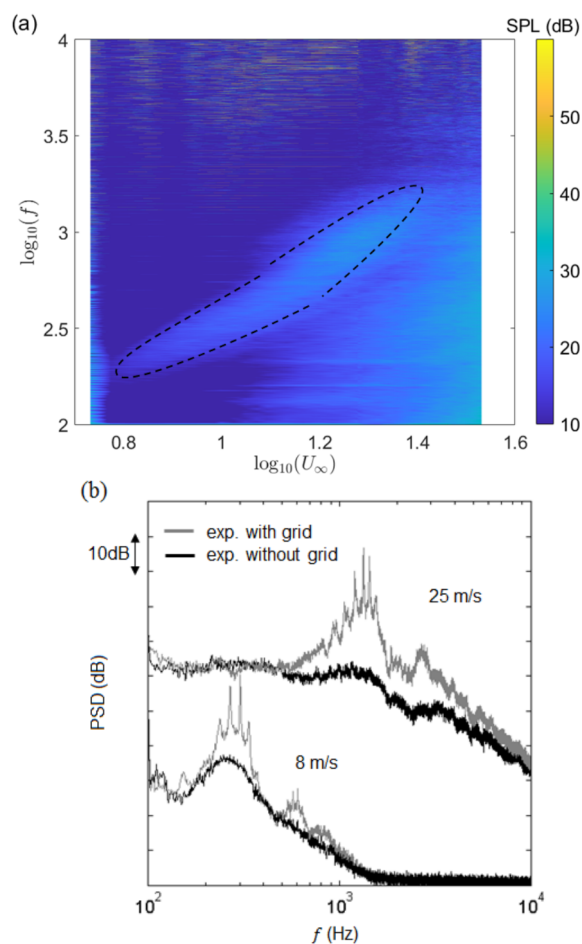


Figure 10. (a) Frequency-flow speed chart for NACA-0012 airfoil at zero AOA with small-scale turbulence; (b) compared far-field sound spectra of the clean flow (grey) and with upstream turbulence (black). Flow speeds 8 m/s and 25 m/s. Both pairs of spectra are shifted by 20 dB from each other [15].

Finally, the cross-spectral analysis [15] of chordwise-located wall-pressure probes (shown in Figure 6) highlighted the highly coherent nature of the fluctuations at the frequencies of the tones and gave access to the convection speed of the instability waves used in AFL analytical predictions. Importantly, the analysis of the spanwise set of probes showed that the tones are associated with essentially two-dimensional unstable motion. This aligns with the above-stated hypothesis of Jones and Sandberg [17] that AFL regularizes the vortex shedding behavior and may be understood as an essentially two-dimensional phenomenon that may be effectively explored using two-dimensional numerical approaches, as will be discussed next.

3.2. Numerical Approaches

Compared to the amount of experimental works, the body of numerical studies focusing on resolving AFL mechanism of airfoil tonal noise production is much less sizeable and expanded relatively recently (clearly, thanks to the advancement of powerful computational resources). Following the DNS study of Desquesnes [16], it included analyses

in [14,17,18,28–30]. Furthermore, the numerical approaches followed in these works almost exclusively rely on high-order finite-difference schemes to solve unsteady, compressible Navier–Stokes equations. The exception is the 3D DNS study of Sanjose et al. [29] that employed lattice Boltzmann method in their analysis (and comparison with experiment) of tonal noise produced by the controlled-diffusion airfoil. The latter approach implemented using the commercial code Powerflow from EXA Corporation offers the convenience of more easily accommodating complex configurations, in particular the effect of impinging wind-tunnel jet flow. The inclusion of the full open-jet wind-tunnel setup as part of computational domain may be essential for proper experimental validation in the cases that involve significant deviation of flow by a loaded (cambered and/or installed at an AOA) airfoil. On the other hand, such approach is often prohibitively expensive, with computations of [29] involving a three-dimensional grid with about 640 million voxels and 10 levels of consecutive grid refinements. Nguyen et al. [30] also realized such approach for AFL analysis of the cambered SD7003 airfoil in a free-jet flow using the same high-order finite-difference approach implemented in [14,18].

3.2.1. Governing Equations for AFL Analysis

To accurately resolve airfoil AFL interactions, a high-fidelity approach is required to solve a set of the compressible unsteady Navier–Stokes equations represented in strong, conservative, time-dependent form in the generalized curvilinear computational coordinates (ξ, η, ζ, τ) transformed from the physical coordinates (x, y, z, t) ,

$$\frac{\partial}{\partial \tau} \left(\frac{\vec{Q}}{J} \right) + \frac{\partial \vec{F}_i}{\partial \xi} + \frac{\partial \vec{G}_i}{\partial \eta} + \frac{\partial \vec{H}_i}{\partial \zeta} + \frac{1}{\text{Re}} \left[\frac{\partial \vec{F}_v}{\partial \xi} + \frac{\partial \vec{G}_v}{\partial \eta} + \frac{\partial \vec{H}_v}{\partial \zeta} \right] = \vec{S} \tag{1}$$

The solution vector $\vec{Q} = (\rho, \rho u, \rho v, \rho w, \rho e)$ is defined in terms of the flow density ρ , Cartesian flow velocity components (u, v, w) , and flow specific energy,

$$e = \frac{T}{\gamma(\gamma - 1)M_\infty^2} + \frac{1}{2}(u^2 + v^2 + w^2) \tag{2}$$

with assumed perfect gas relationship $p = \rho T / \gamma M_\infty^2$ connecting the flow pressure p , temperature T , and the freestream Mach number M_∞ (γ is the specific heat ratio). The other variables in Equation (1) include the inviscid flux vectors defined by,

$$\vec{F}_i = \begin{bmatrix} \rho \hat{u} \\ \rho u \hat{u} + \hat{\xi}_x p \\ \rho v \hat{u} + \hat{\xi}_y p \\ \rho w \hat{u} + \hat{\xi}_z p \\ (\rho e + p) \hat{u} - \hat{\xi}_t p \end{bmatrix}, \quad \vec{G}_i = \begin{bmatrix} \rho \hat{v} \\ \rho u \hat{v} + \hat{\eta}_x p \\ \rho v \hat{v} + \hat{\eta}_y p \\ \rho w \hat{v} + \hat{\eta}_z p \\ (\rho e + p) \hat{v} - \hat{\eta}_t p \end{bmatrix}, \quad \vec{H}_i = \begin{bmatrix} \rho \hat{w} \\ \rho u \hat{w} + \hat{\zeta}_x p \\ \rho v \hat{w} + \hat{\zeta}_y p \\ \rho w \hat{w} + \hat{\zeta}_z p \\ (\rho e + p) \hat{w} - \hat{\zeta}_t p \end{bmatrix} \tag{3}$$

where the transformation Jacobian, $J = \partial(\xi, \eta, \zeta, \tau) / \partial(x, y, z, t)$, the metric quantities defined, e.g., as $\hat{\xi}_x = (J^{-1}) \partial \xi / \partial x$, etc., and the transformed flow velocity components,

$$\begin{aligned} \hat{u} &= \hat{\xi}_t + \hat{\xi}_x u + \hat{\xi}_y v + \hat{\xi}_z w \\ \hat{v} &= \hat{\eta}_t + \hat{\eta}_x u + \hat{\eta}_y v + \hat{\eta}_z w \\ \hat{w} &= \hat{\zeta}_t + \hat{\zeta}_x u + \hat{\zeta}_y v + \hat{\zeta}_z w \end{aligned} \tag{4}$$

The viscous flux vectors, \vec{F}_v, \vec{G}_v and \vec{H}_v , are defined, e.g., in Anderson et al. [31], while \vec{S} represents the source term that, e.g., allows an upstream unsteady vortical perturbation field (such as synthetic turbulence) to be introduced into the flow field analysis. All flow variables are normalized by their respective reference freestream values except for pressure, which is nondimensionalized by $\rho_\infty u_\infty^2$.

Note that the governing equations are represented in the original unfiltered form used unchanged in laminar, transitional, or fully turbulent regions of the flow. The DNS approach (with no modeling of unresolved turbulence scales) was selected in numerical studies of [16,17], while a wall-resolved large-eddy simulation (LES) was implemented in [18,28,30].

3.2.2. Numerical Modeling of Governing Equations

In [17], the employed in DNS numerical algorithm consists of a five-point fourth-order accurate central difference scheme combined with a fourth-order accurate boundary scheme of Carpenter et al. [32] for the spatial discretization, and an explicit fourth-order accurate Runge–Kutta scheme for time-stepping. No artificial viscosity or filtering is used. Instead, as proposed in [33], numerical stability is achieved through appropriate conditioning of the governing equations, such as an entropy-splitting approach for the nonlinear terms, and a Laplacian formulation of the viscous and heat conduction terms. The latter is used to avoid odd–even decoupling when using central finite-difference schemes. In addition, compatible spatial difference operators for the interior and boundary points are employed. Such an approach was also extended in [34] to study TE noise produced by airfoils with serrated and straight flat-plate trailing-edge extensions using an immersed boundary method applied by directly modifying the computational stencil used for discretizing the governing equations in the vicinity of the immersed boundary. Note that a similar task involving 3D analysis of the effect of TE serrations on AFL noise produced by 12% thick Joukowski airfoil was studied using LES in [28].

The AFL numerical analysis of [14,18,30] employed the Implicit LES (ILES) approach developed in [35,36]. In ILES procedure, a high-order low-pass filter operator is applied to the dependent variables during the solution process, in contrast to the standard LES addition of sub-grid stress (SGS) and heat flux terms. The resulting filter selectively damps the evolving poorly resolved high-frequency content of the solution. The ILES code employs a finite-difference approach to discretize the governing equations, with all the spatial derivatives obtained using high-order compact-differencing schemes from [37], with a sixth-order scheme employed in computations of [14,18]. At boundary points, higher-order one-sided formulas are utilized to retain the tridiagonal form of the scheme. In order to ensure that the Geometric Conservation Law (GCL) is satisfied, the time metric terms are evaluated employing the procedures described in detail in [35]. Finally, the time marching is accomplished by incorporating a second-order iterative, implicit, approximately factored procedure as described in [36].

3.2.3. Numerical Implementation

All numerical approaches (both DNS and LES) must use wall-resolved analysis to accurately predict all details of the AFL process, including BL instabilities inception and development before, through, and after LSB, followed by their TE scattering into acoustic waves and propagation of the latter to the point of instabilities inception occurring through BL receptivity process. Such requirement determines a need for extremely high-resolution meshes and correspondingly demanding computational resources. For instance, the fourth-order accurate DNS computations of Jones and Sandberg [17] involved 3125×729 C-mesh grid, yielding approximately 2.3×10^6 grid-points in total.

The sixth-order accurate ILES computations of Nguyen et al. [18] used 1281×789 O-mesh, with the grid carefully clustered near the airfoil surface to achieve the wall-normal and wall-tangent mesh sizes of $\Delta y/c = 2.5 \times 10^{-5}$ and $\Delta x/c = 0.5 \times 10^{-3}$. In terms of the wall units $y_w^+/c = 3.13 \times 10^{-5}$ estimated for the characteristic flow condition with $M = 0.0465$ and $Re = 1.4 \times 10^5$, such grid refinement corresponds to the non-dimensional values of $\Delta y^+ \approx 1$ and $\Delta x^+ = 20$, with 12 grid points clustered in the region $0 < y^+ < 10$. For 3D simulations, such grid parameters correspond to a high-resolution LES according to estimates in [38]. Such grid is also finer compared to the mesh employed in 2D DNS study by Desquesnes et al. [16] that was conducted using the mesh with $\Delta y/c = 3.8 \times 10^{-4}$ and

$\Delta x/c = 6 \times 10^{-3}$. It should be noted that while the use of 2D analysis typically employed in DNS studies could be justified based on the hypothesis of the essentially two-dimensional AFL process, the comparative analysis of 2D vs. 3D approaches conducted in [18] indicates that 2D approach may become misleading. Indeed, the LSB development terminates with the turbulent reattachment occurring close enough to TE but still sufficiently upstream so that the effect of spanwise turbulent redistribution has an impact both on the amplitude and the phase of the vortical structures at TE and the resulting scattered acoustic waves. While such effects will be addressed further below, it should be noted that by comparison, 3D ILES implementation is very computationally demanding due to both increased spatial and time resolution [18]. In all simulations of [18], the steady-state flow conditions were first reached after marching for 20 characteristic cycles to remove all transient processes. The pressure signals were then recorded for over 720,000 time steps, hence for the baseline set-up collecting the data sample for 0.487 sec with the sampling rate of 33.6 kHz, thus achieving the frequency resolution of $\Delta f = 2.05$ Hz.

3.2.4. Linear Stability Analysis

Nearly all the above-mentioned numerical studies of the airfoil AFL interactions employed some form of linear stability analysis (LSA) to complement and compare with numerical data in terms of the predicted evolution of BL instability structures. Such analysis should allow identifying the frequencies of the most amplified instability waves that can be matched against those selected by the AFL process. Essentially, one solves the linearized form of Navier–Stokes equations (e.g., [39]) for the disturbance solution vector ϕ including pressure, velocity, and temperature fluctuations,

$$\phi = (p', u', v', w', T')^T \quad (5)$$

Using a quasi-parallel assumption for the BL time-averaged flow, this vector is described by,

$$\phi(x, y, z, t) = \psi(y)e^{i(\alpha x + \beta z - \omega t)} \quad (6)$$

where ω is the perturbation frequency, β is the spanwise wave number, and α is the streamwise wave number. In the analysis of the spatial evolution of the modes, ω and β are typically specified by the user, and α is the variable of interest in the numerical solution. Assuming a known set of mean flow profiles from numerical simulations or experiment, the linearized Navier–Stokes equations are solved in order to obtain information about the disturbance evolution in the flow. For the current application, a spatial analysis is generally conducted in order to determine the modal growth rate at a given location on the airfoil surface. Therefore, such analysis predicts the values of

$$\alpha = \alpha(\omega, \beta) = \alpha_r + i\alpha_i \quad (7)$$

for a known set of frequencies (e.g., corresponding to the prominent tones in the acoustic and surface pressure spectra), where α_r is the real spatial wavenumber and $-\alpha_i$ determines the instantaneous growth rate at a given streamwise location. Once the growth rates are known at each location, they are integrated along the instability's convection path to obtain the total growth factor N for a disturbance mode at a given frequency defined by,

$$N = \ln\left(\frac{A}{A_0}\right) = \int_{x_0}^x -\alpha_i dx \quad (8)$$

where A_0 is the initial disturbance amplitude, and A is the amplitude of the disturbance at a given streamwise location.

The numerical study of Nguyen et al. [18] employed a linear stability code LAS-TRAC [40] to investigate the BL instability dynamics in NACA-0012 airfoil. As noted in [18], the N -factor in Equation (8) is essentially the normalized accumulated growth

rate of the modal amplitudes integrated over a specified streamwise distance along the boundary layer. The local growth rates of the instability modes thus indicate the slopes of the corresponding N -factor curves. On the other hand, e.g., for the root mean square (RMS) of the flow disturbance pressure P_{RMS} determined from the high-fidelity numerical analysis based on a sample of M selected tonal frequency modes as,

$$P_{RMS}(x) = \sqrt{\frac{1}{M^2} \sum_m |P_m(x)|^2} \quad (9)$$

the slopes of P_{RMS} curves may be easily related to the weighted modal growth rates,

$$dP_{RMS}(x)/dx = \frac{1}{M} \frac{\sum_m (-\alpha_{im}) |P_m(x)|}{\sqrt{\sum_m |P_m(x)|^2}} \quad (10)$$

The connection between the RMS and N -factor curves for the disturbance solution thus becomes evident. In [18], this feature is employed below to match and elucidate results obtained from ILES and LSA analyses in the parametric AFL study.

3.2.5. Numerical Results

The first numerical study revealing the AFL-induced multi-tonal airfoil noise signature was conducted by Desquesnes et al. [16], with the obtained results for the predicted near-field pressure spectrum and BL statistics used as a validation benchmark in subsequent studies. The flow regime with $M = 0.1$ and $Re = 2 \times 10^5$ was considered for NACA-0012 airfoil with the chord of $c = 0.3$ m installed at AOA of 2° . The comparison of the near-field sound pressure spectra predicted in 2D studies [14] and [16] is shown in Figure 11.

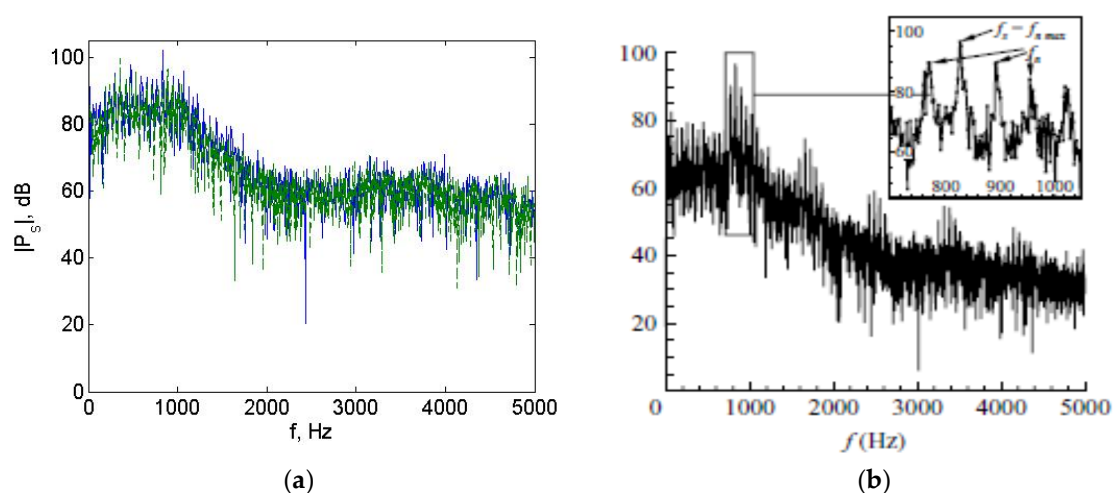


Figure 11. Near-field sound pressure spectra, comparison of [14] (a) and [16] (b). (Adapted from [14]).

The top spectral peaks in Figure 11 manifest the presence of AFL, with multiple tones corresponding to the selected frequencies of the amplified and scattered instability waves. They are present in both analyses but appear sensitive both to the simulation time step and the frequency resolution. Note that high sensitivity of the unsteady data may be indicative of unaccounted, inherently 3D processes taking place in the transitional flow regimes. In a related sense, it also points to the highly nonlinear character of the physical processes involved in the flow-acoustic interactions. In experiments, the intermittency of the radiated tones induced by the TE scattered vortical structures is often witnessed and usually revealed using the spectrogram method wherein the total period of the signal is divided into a number of overlapping bands with the spectral analysis applied to each

band. Figure 12 (bottom plot) illustrates the result of the method applied to the pressure signal extracted from the near-field simulations [14] (that produced the sound spectrum in Figure 11) using 15 bands with 50% overlap. The amplitudes of the present tones vary by color from deep blue to dark red. They appear to fluctuate with time although the main tonal frequency content remains unchanged. Desquesnes et al. [16] also realized the presence of the random component in the computed signal but proved the consistency of the primary tonal spectrum using the related periodogram method based on averaging the results of the Fourier transform applied to each time band.

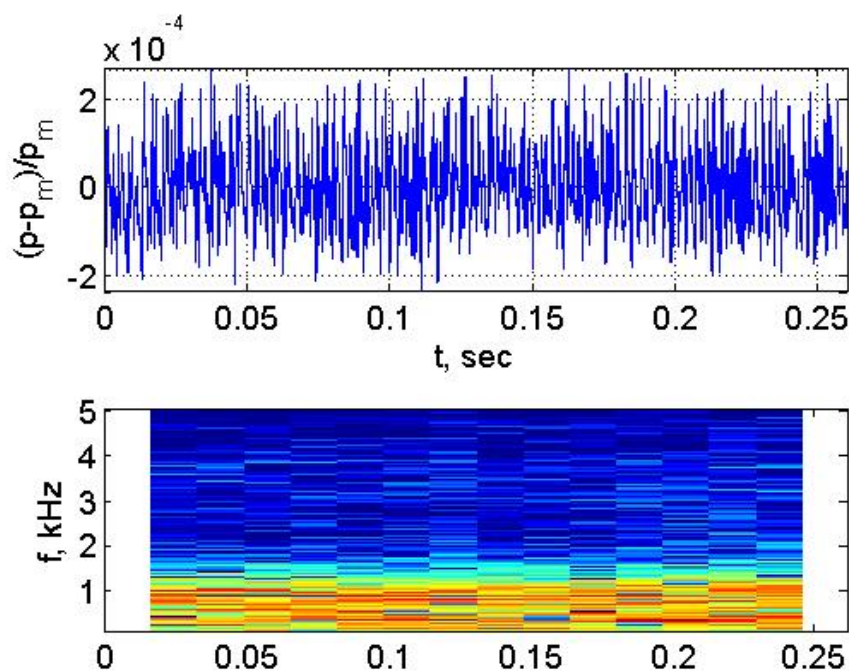


Figure 12. Spectrogram (bottom plot) of the near-field pressure signal (top plot) producing the spectrum in Figure 11. (Adapted from [14]).

The first successful comparison of the predicted sound pressure spectrum against experimental results was presented by Nguyen et al. [18] in the follow-up to the study [14], obtained using the same computational ILES approach. The case study corresponds to the mean flow velocity of 16 m/s ($M = 0.0465$) with uniform upstream flow and $Re = 140,000$ closely representing an experimental condition selected from tests conducted in [14,15]. In Figure 13, the numerical predictions compare well with experiments as peak frequencies are accurately captured and broadband levels are of the same amplitudes at frequencies adjacent to the main tone. Note that 3D ILES results exhibit a near perfect match to experiment between 500–1500 Hz whereas 2D results slightly over-predict the broadband at lower frequencies.

The comparison between 2D and 3D ILES results [18] is further elaborated in Figure 14 showing predicted time-averaged U-velocity contours. Overall, the latter are identical from LE to mid-chord due to the absence of separation and inherently laminar flow. As the flow convects past the mid-chord and travel towards the TE, the differences between the 2D and 3D results become more noticeable as the separation regions and wake structures appear larger from 2D simulations. Figure 15 further illustrates the differences by showing the predicted BL velocity profiles in comparison with experimental measurements [14,15], for selected probe locations.

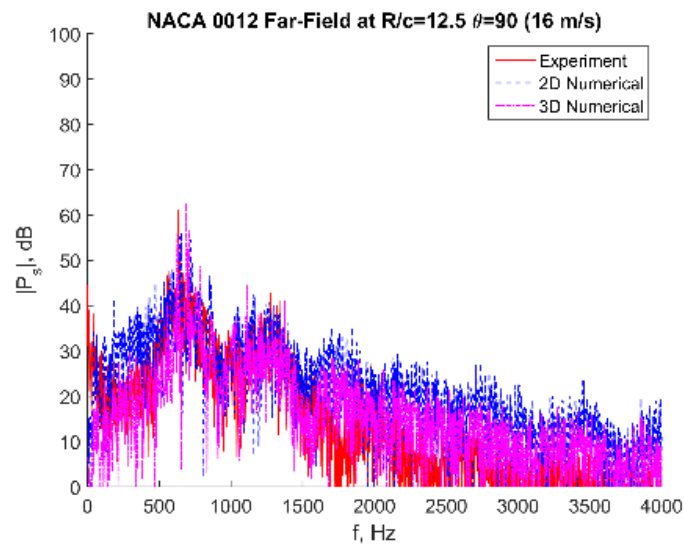


Figure 13. Comparison of 2D (blue) vs. 3D (magenta) vs. measured (red) far-field pressure spectra [18].

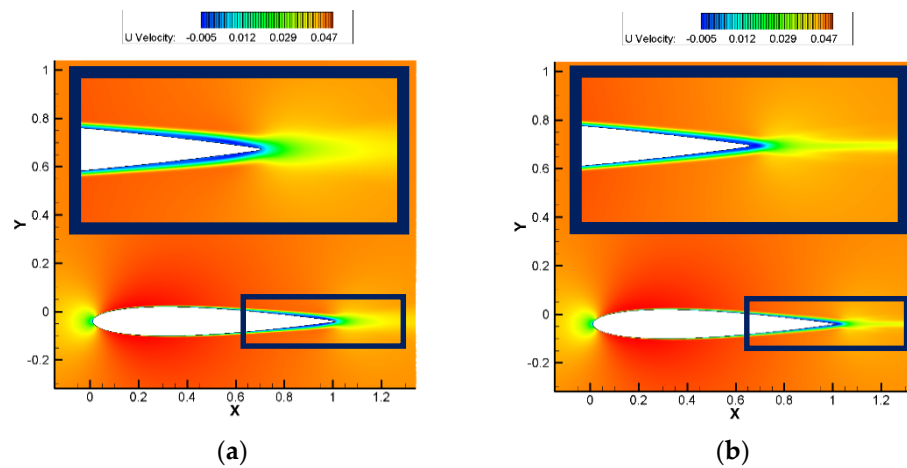


Figure 14. Time-averaged U-velocity contours in 2D (a) and 3D ILES (b). Baseline case for NACA-0012 at 0° AoA and U = 16 m/s [18].

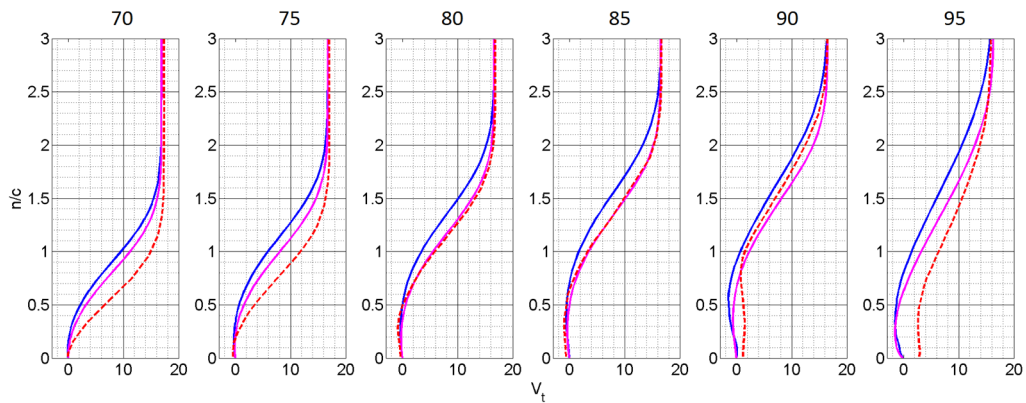


Figure 15. Comparison of 2D (blue) and 3D ILES (magenta) vs. measured (red) suction-side boundary layer profiles. Time-averaged U-velocity, NACA-0012 at 0° AoA and U = 16 m/s [18].

Overall, the above results confirm the validity of utilizing 2D analysis implemented in most AFL studies by revealing a good agreement both with 3D simulations and experimental data. Still, one needs to exercise caution. Figure 16 shows the time snapshots of BL vorticity dynamics based on the detailed 2D vs. 3D ILES comparison conducted in [41] for NACA-0012 airfoil at AOA of 2° , with mean flow velocity of 25 m/sec ($M = 0.072$) and $Re = 180,000$. The results reveal a noticeably different vorticity dynamics on the airfoil suction side caused by the spanwise turbulent energy redistribution and appearance of fine-scale vortical structure in 3D analysis occurring towards the trailing edge.

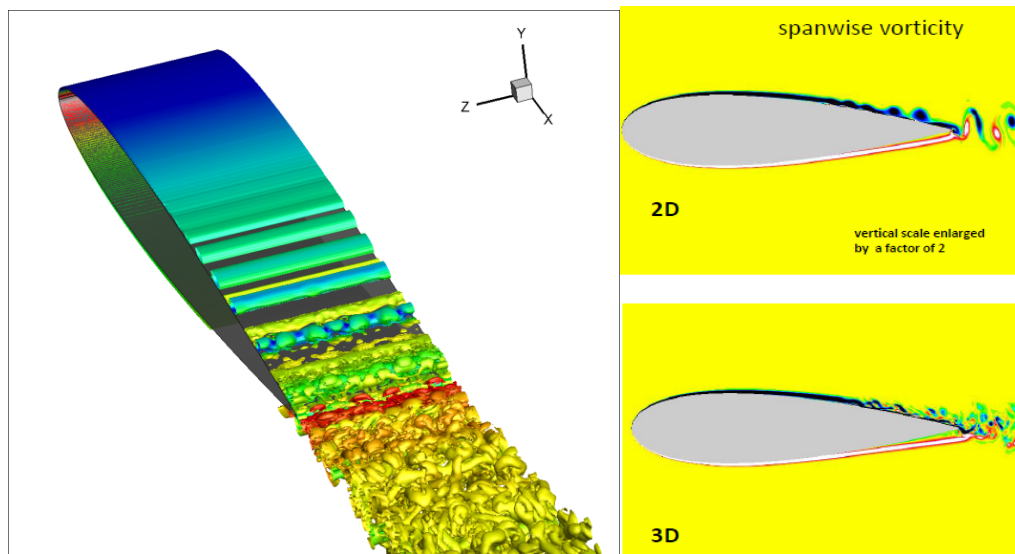


Figure 16. Time snapshots of BL vorticity dynamics from 2D and 3D ILES simulations. NACA-0012 at 2° AoA, $U = 25$ m/s. (Adapted from [41]).

For the same case study, Figure 17 further illustrates the comparison in [41] by also examining grid sensitivity of numerical 2D vs. 3D predictions for two critical parameters: variation of skin friction coefficient c_f indicating suction-side LSB position in terms of BL separation point, and variation of suction-side RMS pressure coefficient $(c_p)_{RMS}$ revealing dynamics of instability structures through and after LSB zone. In the fine-mesh (1285×789) 2D calculations, the separated regions form between $x = 0.5 c$ and $x = 0.75 c$ starting with a very thin separated layer and followed by a near-reattachment point at $x = 0.67$, with a rather short LSB. The results deviate from predictions using the 2D base (643×395) and both 3D meshes, all predicting delayed reattachments with slightly longer LSB zones. Correspondingly, Figure 17b shows that the 2D fine-mesh results predict the rise in RMS pressure slightly further upstream compared to all other computations. The RMS pressure distributions obtained from 2D simulations correspond well with one another and sustain the levels nearly to the trailing edge. This agrees well with other numerical predictions based on 2D analysis [14,16–18], and is identified by the process of slow viscous T-S instability growth before reaching the separation point, followed by transformation of T-S instabilities into inviscid, fast-growing K-H instabilities sustained by LSB's separated sheared layer, and finally their nonlinear saturation through LSB and realization in the form of large-scale vortical rollers (Figure 16). From 2D analysis, such rollers sustain themselves nearly unchanged to the point of TE scattering into acoustic waves. In contrast, 3D results (more grid-sensitive) indicate a rapid decrease of RMS pressure amplitudes after reaching the peak levels, which is again related to the spanwise energy redistribution following the point of turbulent reattachment.

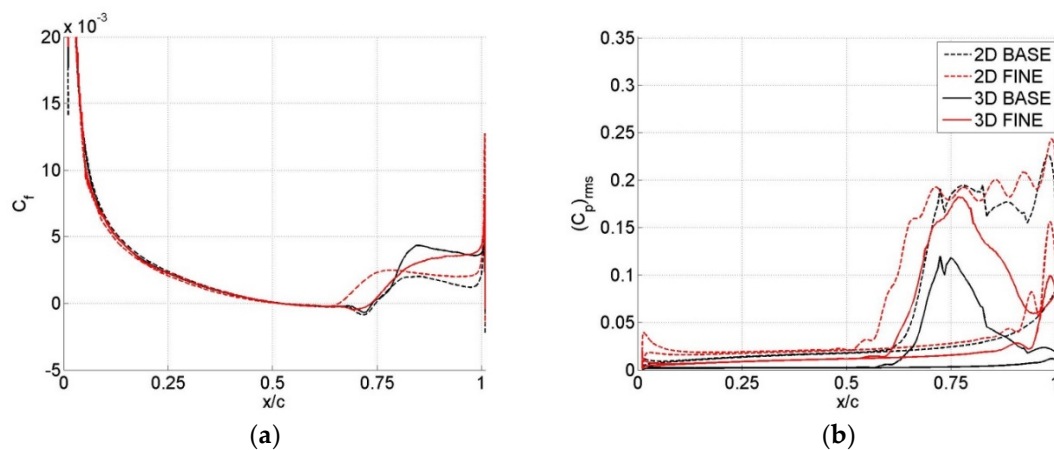


Figure 17. (a) Skin friction coefficient on suction sides. (b) Suction-side airfoil surface RMS pressure distribution. NACA-0012 at 2° AoA, $U = 25$ m/s. (Adapted from [41]).

The effect of upstream turbulence on the disruption of the AFL process was studied numerically in [42] for the same case study using the developed model of synthetic turbulence. In agreement with experimental findings of [14,15] (Figure 10), the high-turbulence results indicated suppression of prominent tones in the surface spectra downstream of the mid-chord location on the suction side, with much higher broadband levels. The analysis of the BL statistical moments indicated that for low-turbulence upstream flow conditions, the LSB was still preserved and flow reattachment occurred without subsequent fully turbulent transition, thus still enabling preservation of the coherent vortical modes and the AFL mechanism. For the high-intensity turbulence case, the much higher RMS disturbance levels were associated with the fully turbulent flow conditions reached on the suction side, with instabilities and the AFL process fully suppressed.

In view of the relationships [9,10], the connection of the above discussed RMS perturbation dynamics with the modal stability analysis is apparent, and further elaborated in the majority of the reviewed studies, albeit primarily from the standpoint of the AFL frequency selection mechanism (discussed in the next section). In [18], the LSA analysis from Section 3.2.4 was applied in conjunction with parametric numerical analysis of NACA-0012 airfoil to investigate transition from tone-producing to no-tone-producing regimes in AOA- Re plane (see Figure 4). By correlating different flow regimes with position and size of LSB on either side of the airfoil, it was determined that at low AoA, distinct tones were present and dominated the acoustics of the airfoil. However, the tones would disappear at higher AoA due to the LSB migration towards the LE and allowing sufficient time for the flow to transition to fully turbulent regime, thus suppressing the AFL mechanism. On the other hand, for a fixed AoA, the increase in flow velocity (Re) was associated with LSB shrinking on the suction side and an increasing dominant contribution of the amplified instabilities on the pressure side (Figure 18) driving the tonal noise production mechanism, which agrees with experimental findings of Yakhina et al. [15] and Pröbsting et al. [22]. The results of LSA analysis [18] correlated with numerical predictions of separated regions for $Re = 144,000$ and for $Re = 288,000$ are illustrated in Figure 19.

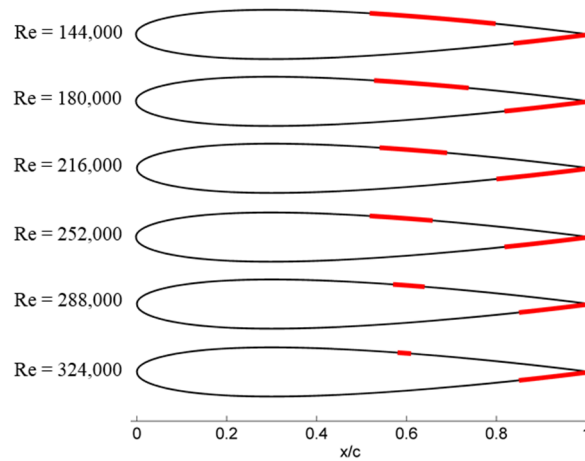


Figure 18. Separation regions with increasing Reynolds number [18].

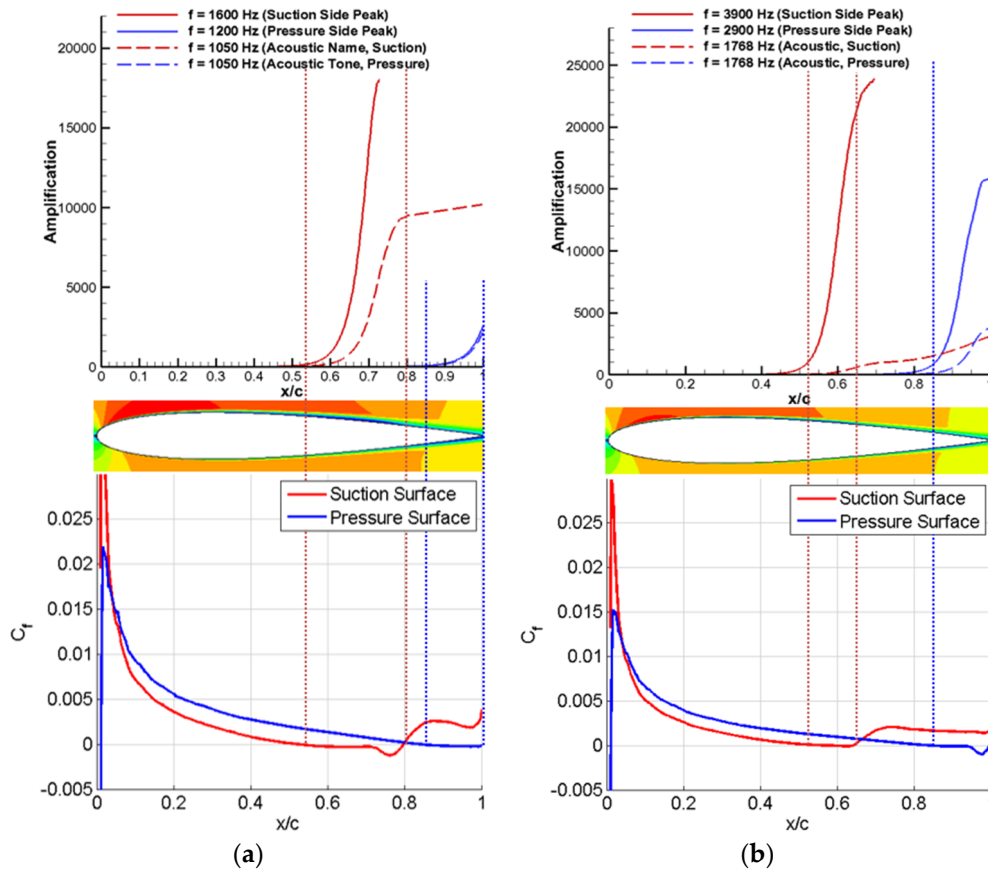


Figure 19. Linear stability analysis (LSA) results (correlated with numerical predictions of laminar separation bubble (LSB) zones) showing instability chordwise amplification on suction and pressure sides for $Re = 144,000$ (a) and $Re = 288,000$ (b) [18].

4. Discussion of AFL Frequency Selection Mechanism and Airfoil Tonal Acoustic Structure

The clustering of equally spaced tones observed in AFL-dominated airfoil acoustic spectra (e.g., in Figure 13) are described by the feedback-loop relationship proposed by Arbey and Bataille [10] in mathematical interpretation of the fact that the convected

BL instabilities must be in phase with coupled acoustic waves at the trailing edge. In application to the AFL scenario suggested by Longhouse [7] in Figure 2, the resulting formula is,

$$f_n \left(\frac{L}{U_c} + \frac{L}{c_0 - U_c} \right) = \left(n + \frac{1}{2} \right) \quad (11)$$

where the tonal frequency f_n is related to the modal number n , distance L between the instability wave inception point (typically, the point of maximum velocity on the surface), the wave convection speed U_c , and the speed of sound c_0 . However, while Equation (11) may help interpret the frequency spacing Δf in the observed cluster of peaks, it does not explain the actual selection of frequencies in the spectrum.

Several studies employed LSA analysis as the primary tool for identifying the AFL frequency selection mechanism and the relationship between the frequencies of the peak radiated acoustic tone and the most amplified instability modes [12,16–18].

Kingan and Pearse [12] developed the method based on that proposed by Nash et al. [11] and McAlpine et al. [43] in order to calculate amplification of T-S instability wave on airfoil surface. They employed XFOIL's [44] mean-flow airfoil solutions to solve Orr-Sommerfeld equation [39], and further combined results with the AFL Equation (11) of Arbey and Bataille [10]. The predicted frequencies agreed reasonably well with experimental data of Paterson et al. [1]. However, [12] also suggested that due to the nonlinear nature of the AFL mechanism, their model cannot relate the level of the produced acoustic tones to instability amplification over the surface. As discussed further, [15] and [17] later proposed and validated such model based on Amiet's TE noise theory using experimental results and numerical predictions, respectively.

Based on their DNS case study of NACA-0012 airfoil in the tone-producing regime with AOA of 2° , $M = 0.1$ and $Re = 200,000$, Desquesnes et al. [16] developed the LSA analysis to match the radiated peak tonal frequency with that of the most amplified instability mode on the pressure side, but not on the suction side. They proposed a complex dual-feedback-loop scenario of multi-tonal acoustic response involving interaction and modulation between pressure and suction side AFLs. However, as has been later experimentally proven using BL trippings (e.g., [14,15]), each side can independently produce the acoustic tonal structure characteristic of AFL interactions.

The DNS analysis of Desquesnes [16] was further extended by Jones and Sandberg [17] for several AOAs between 0° and 2° . When LSA was applied to time-averaged boundary layer profiles, the tonal noise occurred at a frequency significantly lower than that of the most convectively amplified instability wave. Furthermore, with increasing AOA, the most convectively unstable frequency increased significantly while the vortex shedding frequency changed only slightly. The analysis thus revealed that the vortex shedding and acoustic tone observed were not caused directly by convective instability growth, in contrast to the findings in [11,16,43]. The argument was extended to suggest that the vortex shedding behavior while important to noise production, was not directly caused by the AFL process but rather was a result of a global instability that may occur in the absence of AFL, the point certainly in agreement with Tam and Ju [6]. It was also hypothesized that AFL could act as a frequency selection mechanism for the pre-existing vortex shedding behavior, which led to the previously stated argument of AFL "regularizing" the shedding behavior and producing the narrow tonal content when shedding and AFL-selected frequencies matched.

In their parametric study of NACA-0012 airfoil at $Re = 180,000$, Nguyen et al. [18] also considered frequency variation with AOA of the most amplified instability mode and the peak radiated acoustic tone. Figure 20 compares the LSA-predicted frequencies corresponding to the instability waves with maximum amplification (dashed blue lines) against the peak frequencies of calculated acoustic spectra (dashed black lines). In addition, the airfoil surface location where each frequency mode reaches its maximum is shown by the solid green line. Note that for AOA of 0° , the predicted frequency of the most amplified instability mode agrees well with the observed far-field frequency. For other cases, however,

a substantial difference was seen, and was also observed between the predicted peak amplifications for the suction and pressure surfaces. Overall, as the angle of incidence increases, the disparity between the peak LSA-predicted and acoustic tonal frequencies appears to grow. This is illustrated in Figure 21 also showing that the vortex shedding frequency agreed well with the observed acoustic peak tone. Such results are in agreement with those in [17], and it is reasonable to echo some of the scenarios proposed in [17] including the hypothesis of resonant interaction between AFL and shedding mechanisms leading to tonal response with greatly amplified amplitude, compared to the weak pure shedding tone in DNS study of Tam and Ju [6]. It also seems plausible that from the multitude of LSA-identified amplified instability modes, the AFL mechanism described by Equation (11) selects and elevates only those modes in the observed acoustic spectrum that appear the closest to the shedding frequency. We recall that Tam and Ju [6] identified the shedding frequency with that of the most amplified near-wake K-H instability in the free shear layer. The TE scattering of such near-wake instability was claimed as the source of the shedding tone in the absence of AFL. As hypothesized in [18], such wake instability mechanism may superimpose on the AFL mechanism in airfoil tonal noise production, both related to TE scattering of saturated shear-layer vortical structures. To summarize, when the airfoil flow is fully laminar with no AFL present, the remaining shedding tone appears very weak, as demonstrated by Tam and Ju [6]. We have also seen that when the AFL mechanism is suppressed (due to BL tripping or a low-intensity upstream turbulence), the acoustic spectrum still reveals a broadband hump centered around the shedding frequency [14,15]. With the AFL present, the shedding process still provides with the natural selection of the spectral region amplified due to the mutual resonant interference of both mechanisms leading to the observed multi-tonal response.

The above interpretation of the AFL frequency selection mechanism finally allows addressing the dual-ladder-type tonal structure first observed by Paterson et al. [1] (Figure 1). In [18], the results obtained from LSA and numerical predictions over a range of flow velocities were analyzed and compared well (Figure 22) with experimental results of [1,45] to show the expected overlap of the shedding and AFL sound generation mechanisms corresponding to 1.5 and 0.8 in powers of velocity dependence, correspondingly. Furthermore, the dispersion curve analysis was used to extract the convective flow velocity U_c along the airfoil surface and closely match the predicted (using Equation (11)) and ILES-computed tonal frequencies in the reconstructed ladder-type structure.

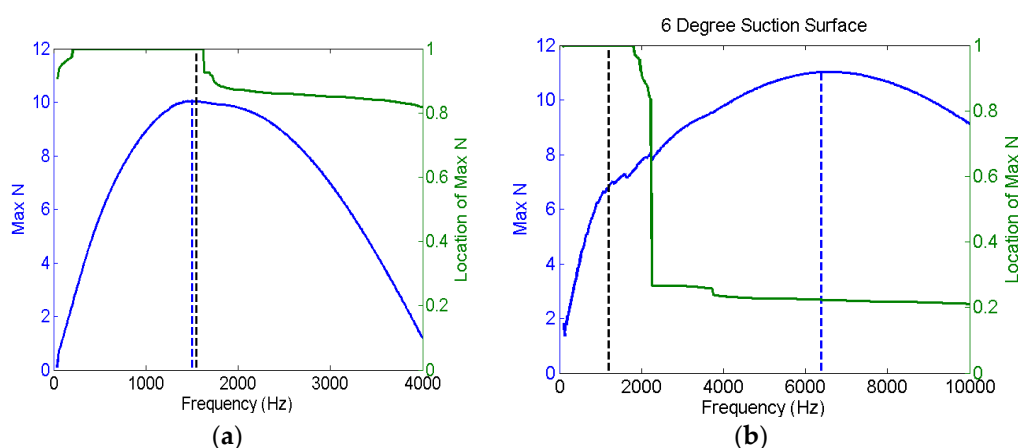


Figure 20. Instability mode amplifications (blue line), location of modal peaks (green line), peak acoustic frequency (dashed black line) for AOA of 0° (a) and 6° (suction side) (b) [18].

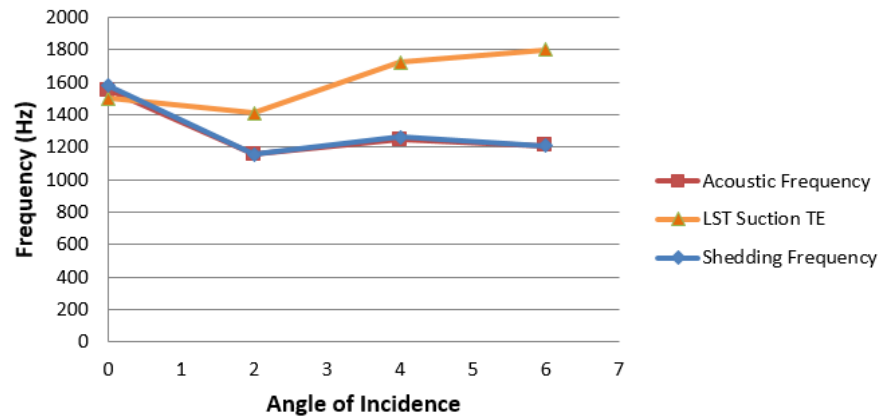


Figure 21. LSA-predicted (triangles), shedding (diamonds), and acoustic (squares) peak frequencies [18].

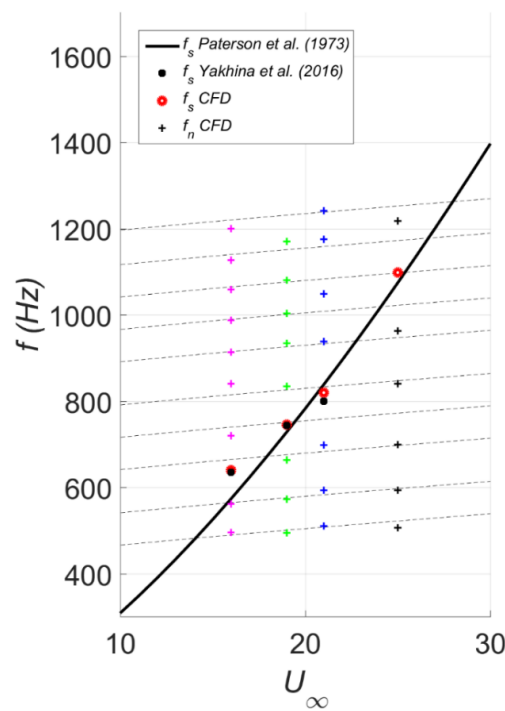


Figure 22. Frequency ladder-type structure generated from numerical simulations [18].

Finally, the analytical predictions of AFL-induced noise are addressed. Note that very few analytical works exist devoted to airfoil AFL mechanism, and in that regard, it is appropriate to mention a study of Atassi [46] considering the AFL existence from the standpoint of connecting TE acoustic scattering with K-H instabilities in a separated airfoil flow, implemented using matched asymptotic expansions.

The analytical predictions of the tonal noise produced by AFL mechanism have been approached using Amiet’s TE noise theory [47]. In [17], the model employed DNS-predicted surface pressure to calculate the radiated dipole-type acoustic directivity that compared well with direct computations (shown in Figure 23 for NACA-0012 airfoil at zero AOA). In [15], the model predictions were based on the measured surface pressure data acquired in the rear part of the airfoil surface and showed an overall satisfactory agreement with the measured tonal levels. These results thus confirmed the cause-to-effect relationship between the AFL-induced airfoil surface pressure and the sound radiated by the airfoil flow-acoustic resonant interactions.

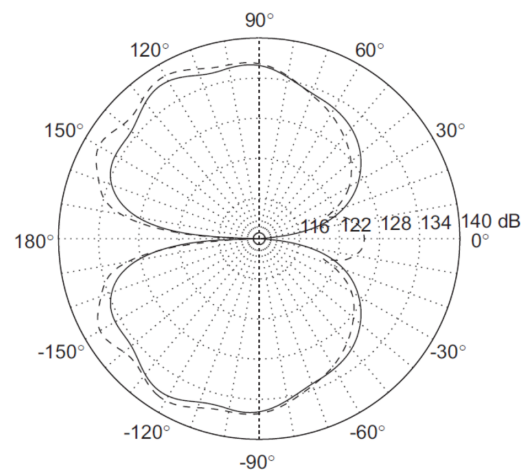


Figure 23. Comparison of acoustic feedback loop (AFL) acoustic directivity obtained from direct numerical simulations (DNS) (dashed line) and predicted using Amiet's trailing edge (TE) noise theory (solid line). (Reprinted from [17], with permission from Elsevier).

5. Conclusions

The last decade has seen a breakthrough in elucidating details of the airfoil AFL process, including the role of LSB and the frequency selection mechanism. Perhaps the most revealing contribution of the reviewed numerical and experimental works is the updated feedback-loop scenario from Longhouse [7] illustrated in Figure 24 [18] that outlines the switch from slowly growing T-S modes (associated with BL viscous effects) to fast-growing inviscid K-H modes (associated with the velocity gradients in the detached LSB shear layer) as a necessary condition for the strong TE acoustic scattering and sustainment of AFL. This, however, is not a sufficient condition since the LSB (on either side of the airfoil) must be located close enough to TE so that the coherent LSB-saturated vortical structures could endure the turbulent reattachment and mixing process disrupting the feedback loop. It was further suggested that AFL could act as a frequency selection mechanism for the pre-existing vortex shedding behavior, “regularizing” the shedding process and producing the strong and narrow tonal content when shedding and AFL-selected frequencies matched. Furthermore, the mutual interaction between the shedding and the AFL mechanisms could select and elevate in the acoustic spectrum those instability modes that are close to the shedding tone which appears naturally through the global instability mechanism. Besides further substantiating the proposed nonlinear interaction scenarios, more studies are still needed to interpret the observed regimes of AFL noise emission such as a switching regime between two tones, a regime with a single tone or two simultaneous tones, and a regime of intermittency with multiple unstable tones.

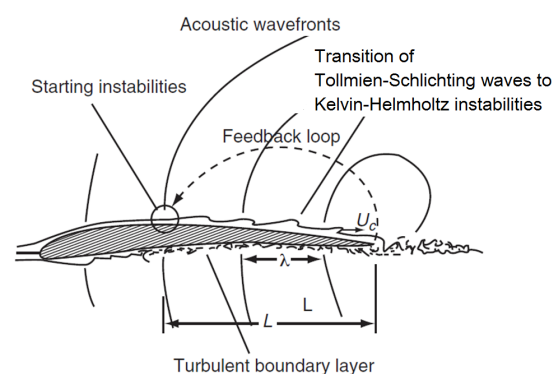


Figure 24. Suggested acoustic feedback loop revised from Longhouse [7,18].

Funding: This research was partially funded by the Air Force Office of Scientific Research (Program Manager D. Smith), grant number FA9550-12-1-0126.

Data Availability Statement: The data presented in this study is openly available in references [1,11,14–18,20,41,45].

Acknowledgments: Partial support for this work through Florida Center for Advanced Aero Propulsion and Plekhanov Russian University of Economics is acknowledged. This publication is also prepared in the implementation of the program for the creation and development of the World-Class Research Center “Supersonic” for 2020–2050 funded by the Ministry of Science and Higher Education of the Russian Federation (Grant agreement of 8 December 2020 № 075-11-2020-023).

Conflicts of Interest: The author declares no conflict of interest.

References

1. Paterson, R.; Vogt, P.; Fink, M.; Munch, C. Vortex noise of isolated airfoils. *J. Aircr.* **1973**, *10*, 296–302. [[CrossRef](#)]
2. Tank, J.; Smith, L.; Spedding, G.R. On the possibility (or lack thereof) of agreement between experiment and computation of flows over wings at moderate Reynolds number. *Interface Focus* **2017**, *7*, 20160076. [[CrossRef](#)] [[PubMed](#)]
3. Yang, S.L.; Spedding, G.R. Local acoustic forcing of a wing at low Reynolds numbers. *AIAA J.* **2014**, *52*, 2867–2876. [[CrossRef](#)]
4. Jones, L.; Sandberg, R.D.; Sandham, N.D. Stability and receptivity characteristics of a laminar separation bubble on an aerofoil. *J. Fluid Mech.* **2010**, *648*, 257–296. [[CrossRef](#)]
5. Tam, C.K.W. Discrete tones of isolated airfoils. *J. Acoust. Soc. Am.* **1974**, *55*, 1173–1177. [[CrossRef](#)]
6. Tam, C.K.W.; Ju, H. Aerofoil tones at moderate Reynolds number. *J. Fluid Mech.* **2012**, *690*, 536–570. [[CrossRef](#)]
7. Longhouse, R.E. Vortex shedding noise of low tip speed axial flow fans. *J. Sound Vib.* **1977**, *53*, 25–46. [[CrossRef](#)]
8. Fink, M.R. Prediction of airfoil tone frequencies. *J. Aircr.* **1975**, *12*, 118–120. [[CrossRef](#)]
9. Schlinker, R.; Amiet, R. Vortex noise from nonrotating cylinders and airfoils. AIAA Paper 1976-81. In Proceedings of the 14th Aerospace Sciences Meeting, Washington, DC, USA, 26–28 January 1976.
10. Arbey, H.; Bataille, J. Noise generated by airfoil profiles placed in a uniform laminar flow. *J. Fluid Mech.* **1983**, *134*, 33–47. [[CrossRef](#)]
11. Nash, E.C.; Lawson, M.V.; McAlpine, A. Boundary-layer instability noise on airfoils. *J. Fluid Mech.* **1999**, *382*, 27–61. [[CrossRef](#)]
12. Kingan, M.J.; Pearse, J.R. Laminar boundary layer instability noise produced by an aerofoil. *J. Sound Vib.* **2009**, *322*, 808–828. [[CrossRef](#)]
13. Plogmann, B.; Herrig, A.; Wurtz, W. Experimental investigations of a trailing edge noise feedback mechanism on a NACA 0012 airfoil. *Exp. Fluids* **2013**, *54*, 1480. [[CrossRef](#)]
14. Golubev, V.V.; Nguyen, L.; Mankbadi, R.R.; Roger, M.; Visbal, M. On flow-acoustic resonant interactions in transitional airfoils. *Int. J. Aeroac* **2014**, *13*, 1–38. [[CrossRef](#)]
15. Yakhina, G.; Roger, M.; Moreau, S.; Nguyen, L.; Golubev, V.V. Experimental and analytical investigation of the tonal trailing-edge noise radiated by low Reynolds number aerofoils. *Acoustics* **2020**, *2*, 293–329. [[CrossRef](#)]
16. Desquesnes, M.; Terracol, M.; Sagaut, P. Numerical investigation of the tone noise mechanism over laminar airfoils. *J. Fluid Mech.* **2007**, *591*, 155–182. [[CrossRef](#)]
17. Jones, L.E.; Sandberg, R.D. Numerical analysis of tonal airfoil self-noise and acoustic feedback loops. *J. Sound Vib.* **2001**, *330*, 6137–6152. [[CrossRef](#)]
18. Nguyen, L.; Golubev, V.V.; Mankbadi, R.R.; Yakhina, G.; Roger, M. Numerical investigation of tonal trailing-edge noise radiated by low Reynolds number airfoils. *Appl. Sci.* **2021**. submitted.
19. Lawson, M.V.; Fiddes, S.P.; Nash, E.C. Laminar boundary layer aeroacoustic instabilities, AIAA Paper 94-0358. In Proceedings of the 32nd Aerospace Sciences Meeting and Exhibition, Reno, NV, USA, 10–13 January 1994.
20. Arcondoulis, E.; Doolan, C.; Zander, A. Airfoil noise measurements at various angles of attack and low Reynolds number. In Proceedings of the ACOUSTICS 2009, Adelaide, Australia, 23–23 November 2009.
21. Inasawa, A.; Kamijo, T.; Asai, M. Generation mechanism of trailing-edge noise of airfoil at low Reynolds numbers. In Proceedings of the 13th Asian Congress of Fluid Mechanics, Dhaka, Bangladesh, 17–21 December 2010.
22. Pröbsting, S.; Scarano, F.; Morris, S. Regimes of tonal noise on an airfoil at moderate Reynolds number. *J. Fluid Mech.* **2015**, *780*, 407–438. [[CrossRef](#)]
23. Pröbsting, S.; Serpieri, J.; Scarano, F. Experimental investigation of aerofoil tonal noise generation. *J. Fluid Mech.* **2014**, *747*, 656–687. [[CrossRef](#)]
24. Pröbsting, S.; Yarusevych, S. Laminar separation bubble development on an airfoil emitting tonal noise. *J. Fluid Mech.* **2015**, *780*, 167–191. [[CrossRef](#)]
25. Chong, T.; Joseph, P.; Kingan, M. An investigation of airfoil tonal noise at different Reynolds numbers and angles of attack. *Appl. Acoust.* **2013**, *74*, 38–48. [[CrossRef](#)]
26. Chong, T.; Joseph, P. Ladder Structure in Tonal Noise Generated Around an Airfoil. *JASA* **2012**, *131*, 1–7. [[CrossRef](#)] [[PubMed](#)]

27. Gerakopoulos, R.; Yarusevych, S. Novel time-resolved pressure measurements on an airfoil at a low Reynolds number. *AIAA J.* **2012**, *50*, 1189–1200. [[CrossRef](#)]
28. Gelot, B.R.; Kim, J.W. Effect of serrated trailing edges on aerofoil tonal noise. *J. Fluid Mech.* **2020**, *904*, A30. [[CrossRef](#)]
29. Sanjose, M.; Towne, A.; Jaiswal, P.; Moreau, S.; Lele, S.; Mann, A. Modal analysis of the laminar boundary layer instability and tonal noise of an airfoil at Reynolds number 150,000. *Int. J. Aeroacoust.* **2019**, *18*, 317–350. [[CrossRef](#)]
30. Nguyen, L.; Golubev, V.; Mankbadi, R.; Roger, M.; Visbal, M. Effect of freejet upstream flow conditions on flow-acoustic resonant interactions in transitional airfoils. AIAA Paper 2016–0052. In Proceedings of the 54th AIAA Aerospace Sciences Meeting, San Diego, CA, USA, 4–8 January 2016.
31. Anderson, D.A.; Tannehill, J.C.; Pletcher, R.H. *Computational Fluid Mechanics and Heat Transfer*; McGraw-Hill Book Company: Philadelphia, PA, USA, 1984.
32. Carpenter, M.H.; Nordstrom, J.; Gottlieb, D. A stable and conservative interface treatment of arbitrary spatial accuracy. *J. Comp. Phys.* **1999**, *148*, 341–365. [[CrossRef](#)]
33. Sandham, N.; Li, Q.; Yee, H. Entropy splitting for high-order numerical simulation of compressible turbulence. *J. Comp. Phys.* **2002**, *178*, 307–332. [[CrossRef](#)]
34. Sandberg, R.D.; Jones, L.E. Direct numerical simulations of airfoil self-noise. *Proc. Eng.* **2010**, *6*, 274–282. [[CrossRef](#)]
35. Visbal, M.R.; Gaitonde, D.V. On the use of high-order finite-difference schemes on curvilinear and deforming meshes. *J. Comp. Phys.* **2002**, *181*, 155–185. [[CrossRef](#)]
36. Visbal, M.R.; Morgan, P.E.; Rizzetta, D.P. An implicit LES approach based on high-order compact differencing and filtering schemes. AIAA Paper 2003-4098. In Proceedings of the 16th AIAA Computational Fluid Dynamics Conference, Orlando, AL, USA, 23–26 June 2003.
37. Lele, S.K. Compact finite difference schemes with spectral-like resolution. *J. Comp. Phys.* **1992**, *103*, 16–42. [[CrossRef](#)]
38. Wagner, C.; Huttl, T.; Sagaut, P. *Large-Eddy Simulation for Acoustics*; Cambridge University Press: Cambridge, UK, 2007.
39. Drazin, P.G.; Reed, W.H. *Hydrodynamic Stability*; Cambridge University Press: Cambridge, UK, 1981.
40. Chang, C. *Langley Stability and Transition Analysis Code (LASTRAC) Version 1.2 User Manual*; NASA/TM-2004-213233; Langley Research Center: Hampton, VA, USA, 2004.
41. Golubev, V.V.; Nguyen, L.; Mankbadi, R.R.; Roger, M.; Visbal, M.R. Acoustic feedback-loop interactions in transitional airfoils. AIAA Paper 2013-2111. In Proceedings of the 19th AIAA/CEAS Aeroacoustics Conference, Berlin, Germany, 27–29 May 2013.
42. Nguyen, L.; Golubev, V.V.; Mankbadi, R.R.; Roger, M.; Pasiliao, C.; Visbal, M.R. Effect of upstream turbulence on flow-acoustic resonance interactions in transitional airfoils. AIAA Paper 2014-3303. In Proceedings of the 20th AIAA/CEAS Aeroacoustics Conference, Atlanta, GA, USA, 16–20 June 2014.
43. McAlpine, A.; Nash, E.C.; Lowson, M.V. On the generation of discrete frequency tones by the flow around an aerofoil. *J. Sound Vib.* **1999**, *222*, 753–779. [[CrossRef](#)]
44. Drela, M. XFOIL: An analysis and design system for low Reynolds number airfoils. In *Low Reynolds Number Aerodynamics*; Lecture Notes in Engineering; Mueller, T.J., Ed.; Springer: Berlin/Heidelberg, Germany, 1989; Volume 54.
45. Yakhina, G.; Roger, M.; Kholodov, P.; Nguyen, L.; Golubev, V.V. An integrated study of laminar separation bubble effect on tonal noise generation in transitional airfoils. AIAA Paper 2016-3022. In Proceedings of the 22nd AIAA/CEAS Aeroacoustics Conference, Lyon, France, 30 May–1 June 2016.
46. Atassi, H.M. Feedback in Separated Flows over Symmetric Airfoils. In Proceedings of the 9th Aeroacoustics Conference, Williamsburg, VA, USA, 15–17 October 1984.
47. Amiet, R. Noise due to turbulent flow past a trailing edge. *J. Sound Vib.* **1976**, *47*, 387–393. [[CrossRef](#)]